Nanoindentation studies of materials

Nanoindentation has become a commonplace tool for the measurement of mechanical properties at small scales, but may have even greater importance as a technique for experimental studies of fundamental materials physics. With high-resolution load-displacement data, discrete events including dislocation source activation, shear instability initiation, and phase transformations can be detected during a nanoindentation test. Recently-developed capabilities in, for example, high-temperature nanoindentation testing and *in situ* imaging of the indented volume, offer new quantitative details about these phenomena, and present many opportunities for future scientific inquiry.

Christopher A. Schuh

Department of Materials Science and Engineering, Massachusetts Institute of Technology, 77 Massachusetts Avenue, Room 8-211, Cambridge, MA 02139 USA
E-mail: schuh@mit.edu

For more than a century, researchers in the mechanical sciences have recognized that surface contacts between materials are highly dependent on their mechanical properties[1,2]. Many different indentation and impression tests have been developed in an effort to measure such mechanical properties from a contact of known geometry. In the past two decades, however, a veritable revolution has occurred in indentation testing, owing to the development of new sensors and actuators that allow instrumented indentations to be routinely performed on submicron scales. The resulting technique, termed *nanoindentation*, has now become ubiquitous for mechanical property measurements at surfaces.

The most common use of nanoindentation is for the measurement of hardness and elastic modulus[3-5], and there has been considerable progress in the measurement of other mechanical parameters as well, including hardening exponents[6-10], creep parameters[11-15], and residual stresses[16-19]. Such measurements have broad application across the physical sciences, and there are several recent reviews on the use of nanoindentation for property extraction[20-22]. However, nanoindentation also lends itself to more fundamental inquiries in materials science. New capabilities in *in situ* and *ex situ* imaging, acoustic emission detection, and high-temperature testing are now being used to probe nanoscale phenomena such as defect nucleation and dynamics, mechanical instabilities or strain localization, and phase transformations. This article presents an overview of nanoindentation's current role and future promise in the study of some of these physical phenomena, with special emphasis on experimental approaches.

Nanoindentation

The principal components in a nanoindentation experiment are the test material, the sensors and actuators used to apply and measure the
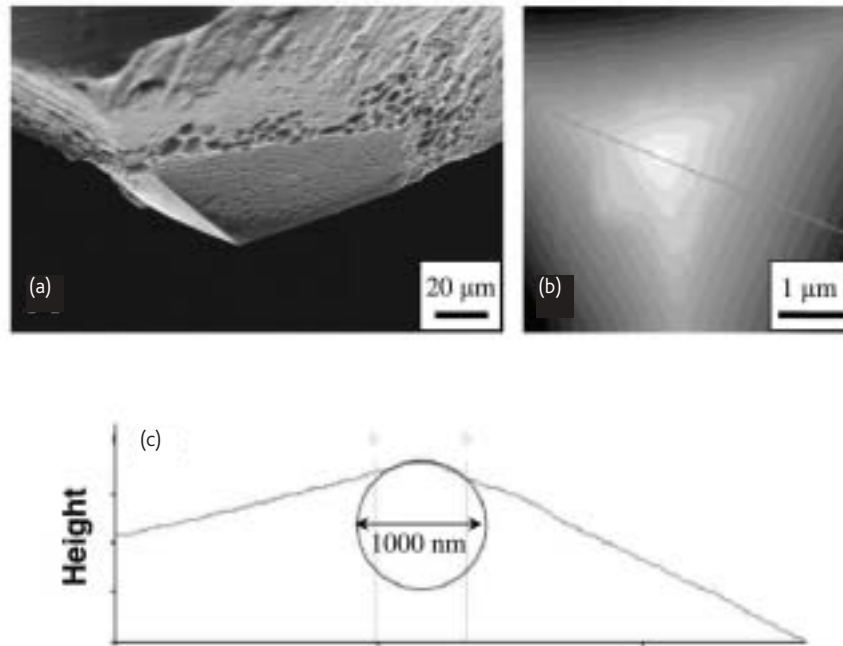
Fig. 1 Views of the Berkovich diamond geometry commonly used in nanoindentation testing. (a) Profile view as observed in a scanning electron microscope, showing the pyramidal diamond tip embedded in a braze. (b) Top–down atomic force microscopy image of the tip, illustrating the three-fold pyramidal symmetry. (c) Line scan height profile of the indenter apex geometry along the line indicated in (b) illustrating the blunting of the apex into a roughly spherical shape with effective diameter ~1000 nm. [Part (a) is courtesy of C. E. Packard and J. R. Trelewicz, Massachusetts Institute of Technology; parts (b) and (c) are reprinted with permission from[38]. © 2002 Elsevier Ltd.]

mechanical load and indenter displacement, and the indenter tip. The latter component is conventionally made of diamond, formed into a sharp, symmetric shape such as the three-sided Berkovich pyramid pictured in Fig. 1. The pyramidal shape is chosen at least in part for its nominal geometric self-similarity, which makes for relatively simpler analysis using the methods of continuum mechanics. However, because of the very fine scale of nanoindentation testing, imperfections in the pyramidal tip shape are of paramount importance in such analysis, and much effort has been focused upon methods of characterizing and cataloging tip shapes for more exact quantitative measurements[3,23-26]. Of particular relevance in this regard is the nature of the tip apex, which is never atomically sharp and exhibits significant blunting, as shown in the atomic force microscope scan of Fig. 1c.

During a typical nanoindentation test, force and displacement are recorded as the indenter tip is pressed into the test material's surface with a prescribed loading and unloading profile. The response of interest is the load-displacement curve (often called the *P-h curve*), such as depicted in Fig. 2 for an indentation on single-crystal Pt(100). The global shape of the *P-h* curve differs from one material to the next, and these variations usually reflect different mechanical properties. Of more interest to the present article are local details in the *P-h* curve, which may signal the operation of discrete physical events beneath the indenter tip.

Fig. 3 shows three examples of *P-h* curves that exhibit interesting local perturbations or discontinuities measured in load-controlled

experiments; these are characteristic of energy-absorbing or energy-releasing events occurring beneath the indenter tip. The three examples shown correspond to three different physical phenomena,
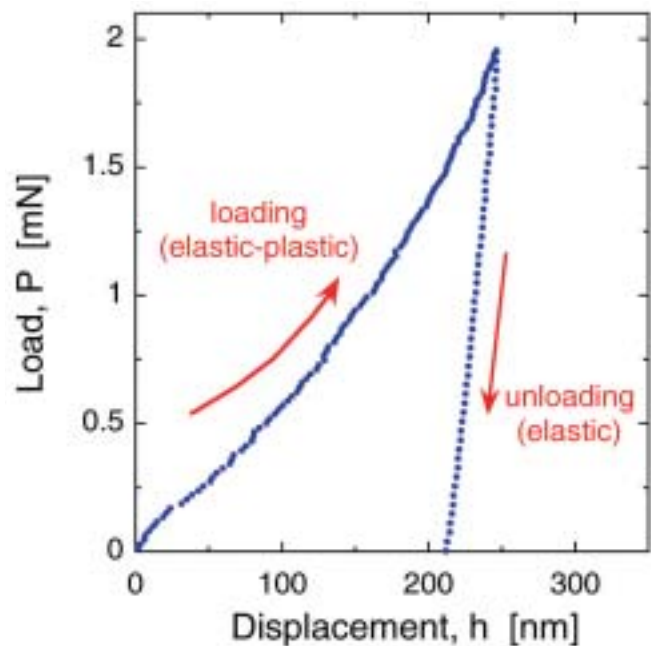

Fig. 2 Example of a typical load-displacement curve (P-h curve) obtained during nanoindentation of an *elastic-plastic material*, in this case single-crystal Pt(100).
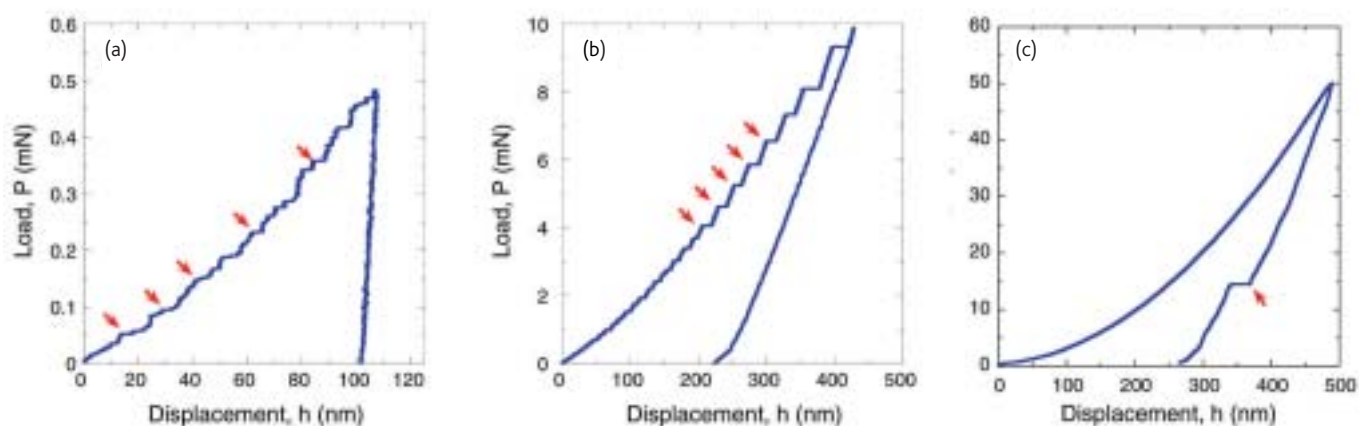
Fig. 3 Three P-h curves that exhibit interesting discontinuities from indentations on (a) pure Pt(100)[27], (b) Pd-Ni-Cu-P metallic glass[28], and (c) single-crystal Si(100)[29]. Some of the relevant discontinuities are indicated by arrows in each case.

in three different materials spanning various states of bonding and structural order:

- Dislocation activity is detected during a shallow indentation into single-crystal Pt[27],
- Shear localization into 'shear bands' is measured in a Pd-based amorphous alloy[28], and
- A phase transformation with a significant volume increase is detected during unloading of an indentation on Si[29].
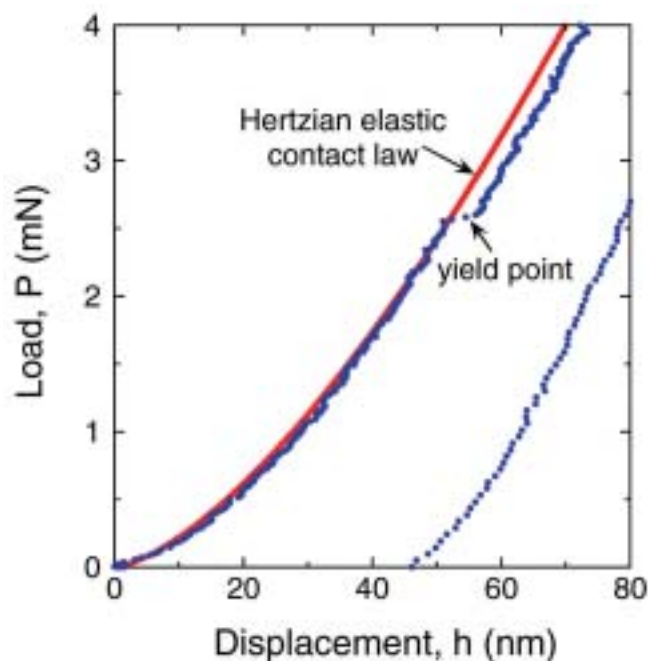

Fig. 4 A load-displacement (P-h) curve for 4H-SiC indented by a roughly spherical tip of ~300 nm radius[46]. The view here is magnified to better illustrate the initial deviation from elastic contact, as predicted using the Hertzian contact law. The yield point corresponds to a discontinuity, or 'pop-in' event.

Because of the very small volume of material sampled in a nanoindentation, these events are detected in a discrete fashion in real time, and can be isolated and studied in detail. In this article, we will focus our attention on the three specific phenomena listed above, although other discrete events (such as fracture or twinning) may be detected during nanoindentation as well.

Incipient plasticity

The largest body of literature using nanoindentation for fundamental materials science is that concerned with the detection and understanding of plastic yield on the nanoscale[30-48], such as for the case of the indentation on pure Pt shown in Fig. 3a. These studies of 'incipient plasticity' often focus upon the very earliest stages of the mechanical contact, where the transition from elastic to plastic deformation can be observed. In this context, the inevitable blunting of the Berkovich tip turns out to be something of a benefit rather than an experimental difficulty; in the earliest stages of contact at which plastic yield first occurs, the geometry of the nanoindenter can often be approximated as spherical. With this fortuitous geometry, it becomes possible to predict the expected elastic response using the Hertzian law for mechanical contacts, based on isotropic continuum elasticity. This law predicts a simple power-law form for the elastic portion of the load-displacement curve, $P \propto h^{3/2}$, with a proportionality constant that is fully specified by the radius of the blunted indenter tip and the elastic properties of the two contacting materials[2]. This expression has been found accurate when compared with the earliest stages of experimental P-h curves from a variety of materials[40-47]. An example from indentations on (0001)-oriented single crystals of 4H-SiC is shown in Fig. 4.

With theoretical expectations for the elastic response given by the Hertzian theory, the onset of plastic deformation during nanoindentation can nominally be identified by the first point at which the experimental data deviate from the elastic curve. In Fig. 4,

Fig. 5 Atomistic simulation result for indentation of Al with a spherical indenter tip, illustrating the nucleation of a dislocation beneath the indented surface[57]. Only miscoordinated atoms are visible, revealing the position of the surface (colored pink and bowed out under the load of the indenter) as well as the first crystal defect that formed at the yield point (colored in blue). (Reprinted courtesy of K. J. Van Vliet, Massachusetts Institute of Technology and with permission from[57]. © 2005 American Physical Society.)

the point of departure is denoted by an arrow. In a great variety of materials, including metals[41,43-45], alloys[40,42], intermetallics[38,49,50], and ceramics[46,51], this yield point has been found to occur at a discontinuity in the *P-h* curve, sometimes referred to as a 'pop-in' event. During this event the indenter travels without a measured increase in applied load (for a load-controlled experiment), or the load is rapidly released at a constant displacement (for a displacement-controlled experiment)[43,52]. Indentations performed to lower, subcritical loads, usually exhibit ideal reversibility and leave no trace of a residual impression on the specimen surface, confirming that the first pop-in marks the onset of irreversible flow. Furthermore, the burst-like character of the first pop-in suggests that strain is accommodated by an abrupt avalanche of atomic activity beneath the indenter, such as might be expected for activation of a dislocation source.

The events that control the first pop-in event during nanoindentation have been the subject of considerable research and remain under active discussion. Details of the atomistic mechanisms behind the pop-in have largely been provided by the simulation community. For example, Kelchner *et al.*[53] first demonstrated via molecular dynamics simulation the possibility that yield may be associated with the homogeneous nucleation of dislocation loops beneath a nanoindentation on pure Au – a result confirmed by many later simulations conducted on various other model materials[37,54-57]. An example of the subsurface nucleation of a crystal defect during simulated nanoindentation of Al is shown in Fig. 5. Some of these simulation efforts have led to considerable quantitative insight into the process of homogeneous dislocation nucleation[57,58]. However, the connection between experiment and simulation remains somewhat tenuous, as simulation time scales are generally several orders of magnitude smaller than in experiments, while the indenter radius usually simulated (~1-10 nm) is much smaller than achieved in experiments (~50-500 nm). A multiscale modeling study by Knap and Ortiz[59] demonstrates the critical effect of this disparity. A 7 nm indenter radius led to homogeneous dislocation nucleation that was easily observed as a discontinuity in the *P-h* curve, while a larger and more realistic tip radius of 70 nm led to considerable dislocation activity without a pop-in event in the *P-h* curve. The implication is that, in experiments, significant undetectable dislocation activity may precede the first pop-in, which would suggest that the pop-in event is not, in fact, a homogeneous dislocation nucleation event, but rather a heterogeneous process of, for example, dislocation source activation or multiplication. In this case, the nominally 'elastic' portion of the *P-h* curve, which fits the predictions of Hertzian contact theory, apparently
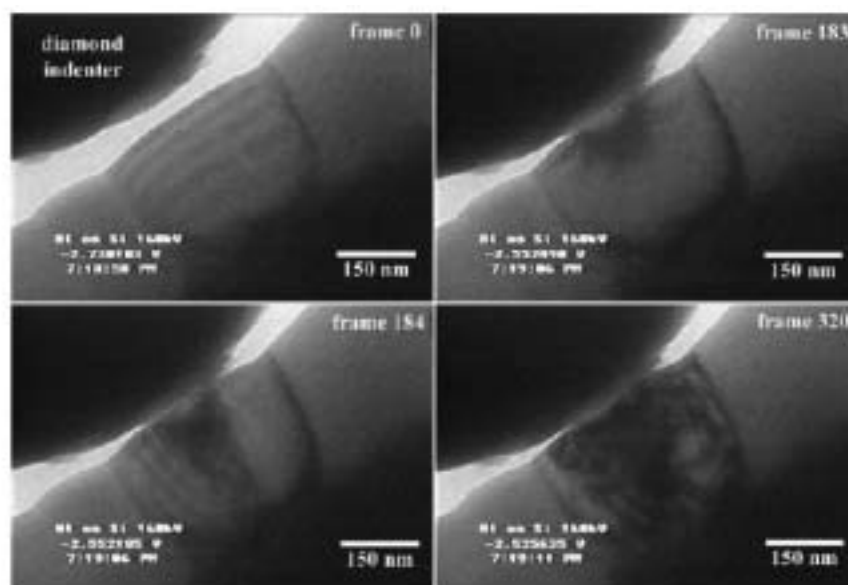

Fig. 6 A series of in situ TEM micrographs from the work of Minor et al.[61], illustrating the response of an Al grain to nanoindentation. In the first frame, the indenter has not yet made contact with the grain below it. The second frame illustrates an elastic contact with strain contours. The third frame is taken just after the first plastic deformation has occurred and lattice dislocations are observed. The fourth frame illustrates the development of a complex dislocation network within the Al grain. (Reproduced with permission from[61]. © 2004 Materials Research Society.)
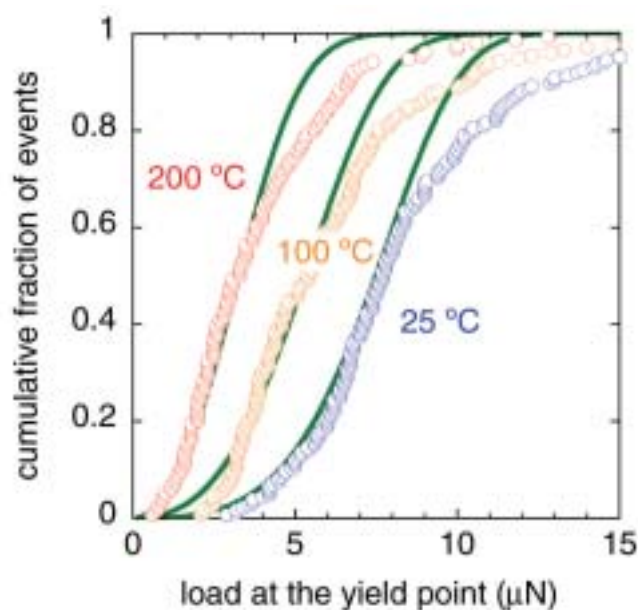
Fig. 7 High-temperature nanoindentation data illustrating the cumulative distribution of measured yield loads for many identical tests performed on the same surface of Pt(110)[65]. As the test temperature increases, the loads required to cause the first pop-in are shifted to lower values, an effect which is consistent with a model for thermally-activated, stress-assisted deformation (green lines).

would contain some amount of superimposed plastic displacement too subtle to detect.

Nanoindentation experiments have not provided nearly as much atomic-level insight into incipient plasticity as have simulations, although new experimental techniques that have emerged in the past few years are quickly remedying this situation[27,60-67]. Minor, Stach, Morris, and coworkers[60-64] have pioneered the development of a hybrid technique incorporating a nanoindenter into a transmission election microscope (TEM), providing *in situ* images of structural evolution beneath an indentation. Fig. 6 shows a series of images from their work on Al[61], where the initial contact with a dislocation-free grain can be observed, followed by the initiation of dislocation activity and the interaction of the dislocation structure with grain boundaries. In a related study, Minor *et al.*[60] showed that the first dislocation activity corresponded closely with a significant discontinuity in the *P-h* curve.

Further quantitative details on the nature of incipient plasticity have also recently been revealed through the use of high-temperature nanoindentation. A number of authors have attempted to extend nanoindentation methods to nonambient conditions in the past decade[14,15,34,68-73], although in general these efforts did not yield sufficient resolution or stability to study the first pop-in in great detail. Some recent approaches have achieved the required conditions for temperatures up to a few hundred degrees centigrade[74,75], and have shown that the first pop-in is thermally activated for at least one metal – Pt[27,65,66].

Fig. 7 demonstrates this effect using a statistical approach, where the same indentation was repeated numerous times at many different locations on the metal surface. The cumulative distribution of pop-in loads measured in this exercise is plotted in Fig. 7, and can be seen to shift as the test temperature is increased; higher temperatures generally lower the load required to initiate yield, a result that conforms with expectations for a thermally activated deformation mechanism. Statistical data such as those in Fig. 7 are also amenable to deeper quantitative analysis[65,66], and have been used to assess the activation energy and activation volume for the yield event in Pt. In the case of a single-crystal Pt surface prepared by electrochemical polishing, such analysis has revealed very low values for both the characteristic energy and volume of the rate-limiting process for yield. This suggests that the first pop-in may be associated with a heterogeneous event, such as the activation of a dislocation source from preexisting surface features or subcritical dislocations.

Development of dislocation networks

Beyond the initial yield point in nanoindentation, additional pop-in events are usually observed at higher loads (see, for example, Fig. 3a for indentation of Pt), which are associated with further dislocation motion, multiplication, and the evolution of a complex defect structure. Such structural evolution is generally quite complicated and varies significantly between materials of different structure, chemistry, and crystallographic orientation. Because of these complexities, analysis of the *P-h* curve alone seems unlikely to yield a detailed physical picture, although imaging of the indented volume, by a variety of techniques, has provided some very useful insights[76-85]. For example, Rojo and coworkers[81-83] have used scanning tunneling microscopy on indented surfaces of (100) Au to reveal the mechanisms by which dislocation activity relocates matter around the impression site. Fig. 8 shows two images of the same surface, after successive indentations placed at the same position. The material ejected during indentation 'piles up' in a
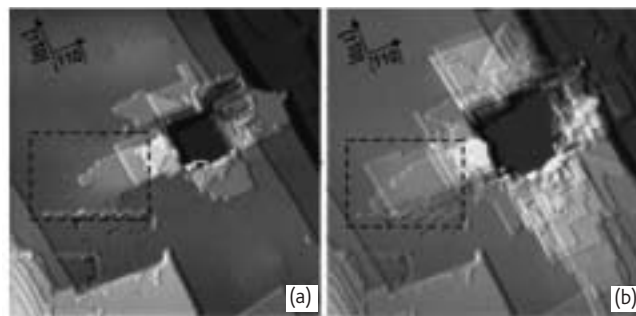

Fig. 8 Scanning tunneling microscope images of a surface of Au(100) after nanoindentation illustrating the redistribution of material around the indentation site. Between frames (a) and (b), the impression was enlarged by indenting on the same location to a higher load. In the dashed box, a stationary screw dislocation can be identified, as well as evidence for the motion of another screw dislocation to create a surface ledge. (Reprinted courtesy of E. Carrasco, O. R. de la Fuente, M. A. González, and J. M. Rojo and with permission from[83]. © 2003 American Physical Society.)
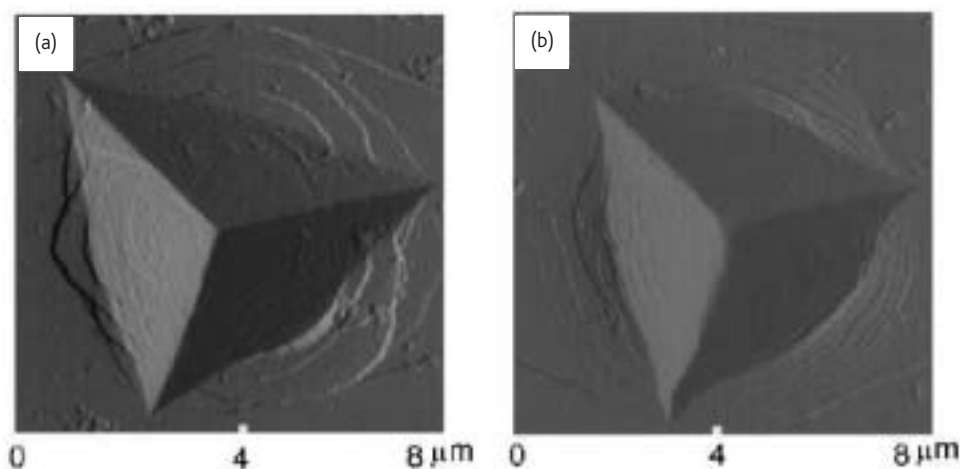
Fig. 9 Atomic force micrographs of nanoindentations in an Al-Fe-Gd metallic glass. Around the three-fold symmetric impression, a series of semicircular shear band traces can be seen. Image (a) illustrates the surface produced after a slow indentation (1 nm/s), while image (b) shows that resulting from a rapid indentation (100 nm/s). (Reproduced courtesy of W. H. Jiang and M. Atzmon and with permission from[92]. © 2003 Materials Research Society.)

series of geometric terraces reflective of the underlying crystal symmetry, and the termination points of some individual screw dislocations can be discerned. The geometry of such surface traces (and the geometry of the impression itself) can be linked to the dislocation slip systems of the crystal. The motion of individual dislocations has been captured by comparing frames such as shown in Fig. 8a and 8b[83].

Mechanical instabilities

In crystalline metals, the motion and mutual interaction of dislocations gives rise to work hardening mechanisms that encourage stable plastic flow. In contrast, in amorphous metals (or metallic glasses) there are no dislocations *per se*, and plastic deformation is inherently unstable, occurring in bursts of highly localized strain referred to as 'shear banding' events. For example, the Berkovich impression shown in Fig. 9a was made on an amorphous Al alloy, and the presence of shear bands is readily observed as a series of steps around the periphery of the indentation.

Nanoindentation testing has recently become an important tool for fundamental studies of shear banding in metallic glasses, owing to its ability to resolve individual shear events under well-controlled conditions[86]. The *P-h* curve for amorphous Pd-Ni-P shown in Fig. 3b is a prototypical response for a metallic glass indented slowly. The loading portion of this curve exhibits an impressive series of pop-in events and, from the earliest such observations[87-89], it has been believed that each of these events correlates with a single shear banding event beneath the indenter. Moser *et al.*[90] recently performed the first *in situ* observation of shear band formation during nanoindentation in a scanning electron microscope and directly correlated pop-in events in the *P-h* curve with the appearance of individual surface steps at the periphery of the indenter.

One of the most quantitatively fruitful approaches to the study of shear bands by nanoindentation has been through the examination of rate and temperature effects on the *P-h* curve. Fig. 10 shows a set of loading curves from the same Pd-Ni-P metallic glass described above, but acquired at different applied loading rates spanning four decades. A transition in the pop-in behavior is observed, with discontinuities becoming fewer and less pronounced as the indentation rate rises. This behavior is typical of many different metallic glasses with widely
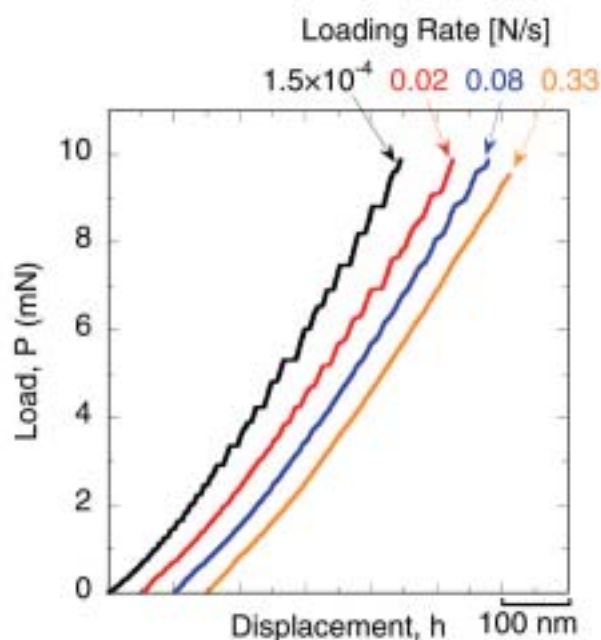

Fig. 10. Typical P-h curves for the loading portion of a nanoindentation test on a Pd-Ni-Cu-P metallic glass[91], offset from one another by 50 nm for clarity of presentation. The number and size of pop-in discontinuities in the curves increases significantly as the indentation rate is lowered.
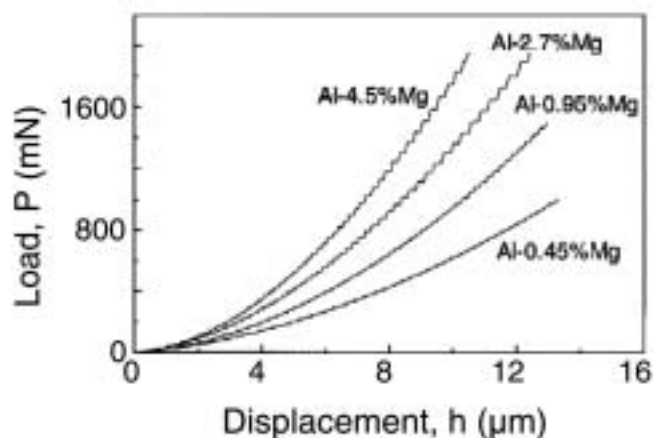
Fig. 11 Load-displacement data acquired during indentation of Al-Mg alloys by Chinh et al.[103] illustrating numerous serrations resulting from mechanical instability. The concentration dependence of this phenomenon can also be observed by comparing the different curves. (Reproduced courtesy of N. Q. Chinh, F. Csikor, Zs. Kovács, and J. Lendvai and with permission from[103]. © 2000 Materials Research Society.)

different chemical compositions, and has been documented by a number of authors working with a variety of different nanoindenters[28,74,89,91-95]. The rate effect is also associated with a shift in the distribution of shear band traces on the surface of the material. Figs. 9a and 9b compare indentations performed at relatively lower and higher rates, respectively, from which it is clear that faster indentations produce a higher number density of more closely-spaced shear bands.

Quantitative analysis of these kinds of *P-h* data has led to significant insight into the process of shear localization in metallic glasses. For example, a collection of high-temperature experiments[74] was used to identify a 'critical' submicron-scale size for shear banding, below which strain is localizing and the shear band is growing, and above which strain has completely localized into the now rapidly propagating shear band. In complementary work combining indentation with *ex situ* TEM observations, other researchers have studied deformation-induced structural evolution and nanocrystallization events in metallic glasses[86,96-98]. These various studies represent initial efforts in the exploration of a very complex topic, and there is not yet broad agreement as to the mechanisms of shear localization in metallic glasses, or how the glass structure and structural evolution impacts the deformation. Nonetheless, these kinds of studies clearly represent an avenue for significant scientific advances in the future.

Shear banding in amorphous metals is just one example of a mechanical instability that can be studied using nanoindentation, and similar instabilities in other materials are amenable to the same kinds of experimental approaches. A good example of this is the so-called 'jerky flow' of solid solution alloys, which has recently been considered by Chinh *et al.*[99-104] using depth-sensing indentation. Sample data for Al-Mg alloys acquired by this group are shown in Fig. 11, which shows *P-h* curves with various degrees of flow serration

beneath the indenter. The instability that gives rise to discontinuities in this case results from the interaction of lattice dislocations with solute atoms, which leads to instantaneous negative strain rate sensitivity and localization of flow. Chinh *et al.* have used data such as these to study the statistics of flow serration, as well as the influence of solute concentration on the instability.

Phase transformations

Many materials undergo phase transformations when subjected to large hydrostatic stresses, and the pressure beneath a nanoindenter is generally quite high (on the order of several gigapascals). In the case of some diamond-cubic semiconductors – including Si and Ge – the mean contact pressure of hardness indentations closely matches the critical pressure to trigger a structural transformation[105-107]. The interest in indentation-induced phase transformations has been steadily increasing for decades, and the wide adoption of nanoindentation techniques has spurred further study.

The *P-h* curve shown in Fig. 3c is a typical example of the indentation response seen in Si for relatively high loads[29]. When sharp indentation impressions are examined *ex situ*, thin sheets of material extruded around the periphery of the indenter can be observed, as shown in Fig. 12[29,108,109]. This extensive plastic flow has been interpreted as evidence for the transformation from diamond cubic Si to the metallic (and malleable) β-Sn phase under the pressure of the indentation[108,109]. More direct evidence for a semiconducting/metallic transition under the indenter has also been provided by *in situ* electrical measurements performed by several authors[106,107,110,111].

The sequence of events during the unloading portion of an indentation are less clearly resolved, although the problem has been studied extensively[29,84,110,112-122]. Various *ex situ* TEM and Raman spectroscopy studies have been conducted, and an impressive number of polymorphs appear to be involved – eight or more in Si, seven or more in Ge – depending upon the indenter shape, applied load, and rate of unloading. These effects have been summarized by Domnich and Gogotsi[122], who extensively reviewed the literature up to 2001.
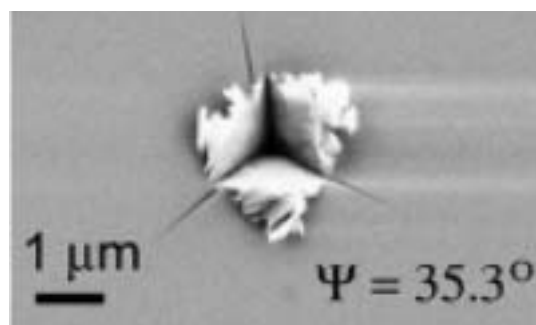

Fig. 12. Scanning electron micrograph of a cube-corner geometry indentation on Si(100) illustrating a copious amount of sheet-like material that has been extruded out from beneath the indenter; this is taken as evidence of pressure-induced transformation to a plastic metallic state during indentation[29]. (Reproduced with permission from[29]. © 2005 Elsevier Ltd.)
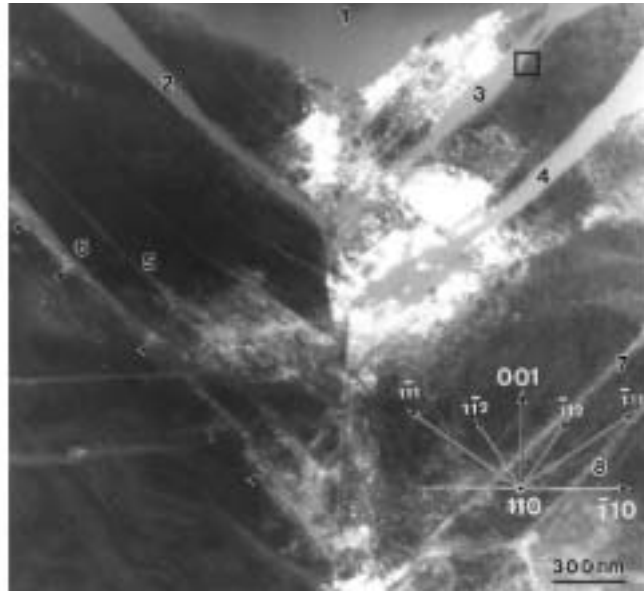
Fig. 13 Dark-field TEM image showing a cross-sectional view of indented Si [123]. The regions labeled 1-4 are amorphous and the bands 2-4 are aligned with the expected slip planes in diamond-cubic Si. (Reproduced with permission from[123]. © 2002 Taylor and Francis, Ltd.)

The pop-out phenomenon observed during unloading in Fig. 3c is attributed to the reversion of the high-pressure β-Sn phase to metastable rhombohedral or body-centered cubic phases[121]. The transformation carries an attendant increase in volume that can do mechanical work against the indenter tip, producing the pop-out effect.

The presence of amorphous regions after indentation of Si has been widely observed in TEM studies[84,114-118,123], and represents an interesting departure from the equilibrium phase diagram. Although several authors have suggested that deviatoric stresses or plastic deformation may impact the evolution of metastable phases under the indenter, this remains an area where additional work is required. For example, Tachi Suprijadi *et al.*[123] have used *ex situ* cross-sectional TEM to observe the structure of indented Si, and identified amorphous bands aligned with the expected slip systems for the diamond-cubic structure (Fig. 13). This hints at the involvement of plastic flow in the transformation sequence beneath the indenter, which is not captured by static equilibrium arguments alone. Thus, nanoindentation may offer the possibility of studying nonequilibrium phase transformations (so-called 'driven' transformations) with new levels of consistency and control.

Summary

Nanoindentation presents considerable potential for understanding discrete atomic rearrangements under stress, ranging from phase transformations in small volumes of material to the motion and formation of individual defects such as lattice dislocations or shear bands. By itself, nanoindentation often allows the detection of such events under a reasonably well-defined stress state. When the technique is augmented by additional capabilities, such as a high-temperature testing stage, *in situ* electron microscopy, or *ex situ* measurements by scanning probe microscopy or Raman spectroscopy, near-atomic level details of deformation physics can be deduced. As these techniques become more refined and their synergy with nanoindentation equipment improves, it is expected that the resulting experimental data will play a key role in the development of consistent theories of material behavior at the nanoscale. mt

Acknowledgments

REFERENCES

1. Timoshenko, S. P., *History of Strength of Materials*, McGraw-Hill, New York, (1953)
2. Johnson, K. L., *Contact Mechanics*, Cambridge University Press, UK (1985)
3. Oliver, W. C., and Pharr, G. M., *J. Mater. Res.* (1992) **7**, 1564
4. Oliver, W. C., and Pharr, G. M., *J. Mater. Res.* (2004) **19**, 3
5. Bhushan, B., In *Handbook of Micro/Nano Tribology*, Bhushan, B., (ed.) CRC Press, Boca Raton, Florida (1999), 433
6. Dao, M., *et al.*, *Acta Mater.* (2001) **49**, 3899
7. Chollacoop, N., *et al.*, *Acta Mater.* (2003) **51**, 3713
8. Bucaille, J. L., *et al.*, *Acta Mater.* (2003) **51**, 1663
9. Kucharski, S., and Mróz, Z., *Mater. Sci. Eng. A* (2001) **318**, 65
10. Ma, D., *et al.*, *J. Appl. Phys.* (2003) **94**, 288
11. Fischer-Cripps, A. C., *Mater. Sci. Eng. A* (2004) **385**, 74
12. Oyen, M. L., and Cook, R. F., *J. Mater. Res.* (2003) **18**, 139
13. Storåkers, B., and Larsson, P.-L., *J. Mech. Phys. Solids* (1994) **42**, 307

14. Lucas, B. N., and Oliver, W. C., *Metall. Mater. Trans. A* (1999) **30**, 601
15. Takagi, H., *et al.*, *Philos. Mag.* (2003) **83**, 3959
16. Suresh, S., and Giannakopoulos, A. E., *Acta Mater.* (1998) **46**, 5755
17. Carlsson, S., and Larsson, P.-L., *Acta Mater.* (2001) **49**, 2179
18. Carlsson, S., and Larsson, P.-L., *Acta Mater.* (2001) **49**, 2193
19. Swadener, J. G., *et al.*, *J. Mater. Res.* (2001) **16**, 2091
20. Cheng, Y.-T., and Cheng, C.-M., *Mater. Sci. Eng. R* (2004) **44**, 91
21. Fischer-Cripps, A. C., *Nanoindentation*, Springer, New York, USA (2002)
22. VanLandingham, M. R., *J. Res. Natl. Inst. Stand. Technol.* (2003) **108**, 249
23. Thurn, J., and Cook, R. F., *J. Mater. Res.* (2002) **17**, 1143
24. VanLandingham, M. R., *et al.*, *Measurement Sci. Technol.* (2005) **16**, 2173
25. McElhaney, K. W., *et al.*, *J. Mater. Res.* (1998) **13**, 1300
26. Meneve, J. L., *et al.*, *Appl. Surf. Sci.* (1996) **101**, 64
27. Lund, A. C., *et al.*, *Appl. Phys. Lett.* (2004) **85**, 1362
28. Schuh, C. A., and Nieh, T. G., *Acta Mater.* (2003) **51**, 87
29. Jang, J. I., *et al.*, *Acta Mater.* (2005) **53**, 1759
30. Gane, N., and Bowden, F. P., *J. Appl. Phys.* (1968) **39**, 1432
31. Gerberich, W. W., *et al.*, *Acta Metall. Mater.* (1995) **43**, 1569
32. Mann, A. B., and Pethica, J. B., *Appl. Phys. Lett.* (1996) **69**, 907
33. Corcoran, S. G., *et al.*, *Phys. Rev. B* (1997) **55**, R16057
34. Bahr, D. F., *et al.*, *J. Mater. Res.* (1999) **14**, 2269
35. Mann, A. B., *Philos. Mag. A* (1999) **79**, 577
36. Tymiak, N. I., *et al.*, *Acta Mater.* (2001) **49**, 1021
37. Li, J., *et al.*, *Nature* (2002) **418**, 307
38. Chiu, Y. L. , and Ngan, A. H. W., *Acta Mater.* (2002) **50**, 1599
39. Shibutani, Y., and Koyama, A., *J. Mater. Res.* (2004) **19**, 183
40. Gerberich, W. W., *et al.*, *Acta Mater.* (1996) **44**, 3585
41. Michalske, T. A., and Houston, J. E., *Acta Mater.* (1998) **46**, 391
42. Bahr, D. F., *et al.*, *Acta Mater.* (1998) **46**, 3605
43. Kiely, J. D., and Houston, J. E., *Phys. Rev. B* (1998) **57**, 12588
44. Suresh, S., *et al.*, *Scripta Mater.* (1999) **41**, 951
45. Gouldstone, A., *et al.*, *Acta Mater.* (2000) **48**, 2277
46. Schuh, C. A., and Lund, A. C., *J. Mater. Res.* (2004) **19**, 2152
47. Bahr, D. F., and Vasquez, G., *J. Mater. Res.* (2005) **20**, 1947
48. Pethica, J. B., and Tabor, D., *J. Adhesion* (1982) **13**, 215
49. Chiu, Y. L., and Ngan, A. H. W., *Acta Mater.* (2002) **50**, 2677
50. Wang, W., *et al.*, *Acta Mater.* (2003) **51**, 6169
51. Wang, X., and Padture, N. P., *J. Mater. Sci.* (2004) **39**, 1891
52. Warren, O. L., *et al.*, *Z. Metallkd.* (2004) **95**, 287
53. Kelchner, C. L., *et al.*, *Phys. Rev. B* (1998) **58**, 11085
54. Lilleodden, E. T., *et al.*, *J. Mech. Phys. Solids* (2003) **51**, 901
55. Zhu, T., *et al.*, *J. Mech. Phys. Solids* (2004) **52**, 691
56. Miller, R. E., *et al.*, *Acta Mater.* (2004) **52**, 271
57. Van Vliet, K. J., *et al.*, *Phys. Rev. B* (2003) **67**, 104105
58. Ronald, R. E., *J. Mech. Phys. Solids* (2004) **52**, 1507
59. Knap, J., and Ortiz, M., *Phys. Rev. Lett.* (2003) **90**, 226102
60. Minor, A. M., *et al.*, *Appl. Phys. Lett.* (2001) **79**, 1625
61. Minor, A. M., *et al.*, *J. Mater. Res.* (2004) **19**, 176
62. Ohmura, T., *et al.*, *J. Mater. Res.* (2004) **19**, 3626
63. Soer, W. A., *et al.*, *Acta Mater.* (2004) **52**, 5783
64. Minor, A. M., *et al.*, *Philos. Mag.* (2005) **85**, 323
65. Schuh, C. A., *et al.*, *Nature Mater.* (2005) **4**, 617
66. Mason, J. K., *et al.*, *Phys. Rev. B* (2006) **73**, 054102
67. Tymiak, N. I., *et al.*, *Acta Mater.* (2004) **52**, 553
68. Farber, B. Ya., *et al.*, *Philos. Mag. A* (1998) **78**, 671

69. Syed-Asif, S. A., and Pethica, J. B., *Philos. Mag. A* (1997) **76**, 1105
70. Smith, J. F., and Zheng, S., *Surf. Eng.* (2000) **16**, 143
71. Beake, B. D., and Smith, J. F., *Philos. Mag. A* (2002) **82**, 2179
72. Beake, B. D., *et al.*, *Z. Metallkd.* (2003) **94**, 798
73. Volinsky, A. A., *et al.*, *J. Mater. Res.* (2004) **19**, 2650
74. Schuh, C. A., *et al.*, *Acta Mater.* (2004) **52**, 5879
75. Schuh, C. A., *et al.*, *J. Mater. Res.* (2006) **21**, 725
76. Rabe, R., *et al.*, *Thin Solid Films* (2004) **469–470**, 206
77. Viswanathan, G. B., *et al.*, *Acta Mater.* (2005) **53**, 5101
78. Nibur, K. A., and Bahr, D. F., *Scripta Mater.* (2003) **49**, 1055
79. Gaillard, Y., *et al.*, *Philos. Mag. Lett.* (2003) **83**, 553
80. Gaillard, Y., *et al.*, *Acta Mater.* (2003) **51**, 1059
81. de la Fuente, O. R., *et al.*, *Phys. Rev. Lett.* (2002) **88**, 036101
82. de la Fuente, O. R., *et al.*, *Philos. Mag.* (2003) **83**, 485
83. Carrasco, E., *et al.*, *Phys. Rev. B* (2003) **68**, 180102
84. Page, T. F., *et al.*, *J. Mater. Res.* (1992) **7**, 450
85. Stelmashenko, N. A., *et al.*, *Acta Metall. Mater.* (1993) **41**, 2855
86. Schuh, C. A., and Nieh, T. G., *J. Mater. Res.* (2004) **19**, 46
87. Wang, J. G., *et al.*, *J. Mater. Res.* (2000) **15**, 798
88. Golovin, Yu. I., *et al.*, *Scripta Mater.* (2001) **45**, 947
89. Schuh, C. A., *et al.*, *J. Mater. Res.* (2002) **17**, 1651
90. Moser, B., *et al.*, *Adv. Eng. Mater.* (2005) **7**, 388
91. Schuh, C. A., *et al.*, *Philos. Mag.* (2003) **83**, 2585
92. Jiang, W. H., and Atzmon, M., *J. Mater. Res.* (2003) **18**, 755
93. Concustell, A., *et al.*, *J. Mater. Res.* (2005) **20**, 2719
94. Nieh, T. G., *et al.*, *Intermetallics* (2002) **10**, 1177
95. Zhang, G. P., *et al.*, *Scripta Mater.* (2005) **52**, 1147
96. Kim, J.-J., *et al.*, *Science* (2002) **295**, 654
97. Jiang, W. H., *et al.*, *J. Appl. Phys.* (2003) **93**, 9287
98. Kramer, M. J., *et al.*, *J. Non-Cryst. Solids* (2005) **351**, 2159
99. Bérces, G., *et al.*, *J. Mater. Res.* (1998) **13**, 1411
100. Chinh, N. Q., *et al.*, *Mater. Sci. Eng. A* (2002) **324**, 219
101. Bérces, G., *et al.*, *Acta Mater.* (1998) **46**, 2029
102. Bérces, G., *et al.*, *J. Mater. Res.* (1998) **13**, 1411
103. Chinh, N. Q., *et al.*, *J. Mater. Res.* (2000) **15**, 1037
104. Chinh, N. Q., *et al.*, *J. Mater. Res.* (2004) **19**, 31
105. Gerk, A. P., and Tabor, D., *Nature* (1978) **271**, 732
106. Clarke, D. R., *et al.*, *Phys. Rev. Lett.* (1988) **60**, 2156
107. Gridneva, I. V., *et al.*, *Phys. Status Solidi A* (1972) **14**, 177
108. Pharr, G. M., *et al.*, *J. Mater. Res.* (1991) **6**, 1129
109. Kailer, A., *et al.*, *J. Appl. Phys.* (1997) **81**, 3057
110. Mann, A. B., *et al.*, *J. Mater. Res.* (2000) **15**, 1754
111. Bradby, J. E., *et al.*, *Phys. Rev. B* (2003) **67**, 085205
112. Zarudi, I., *et al.*, *J. Mater. Res.* (2003) **18**, 758
113. Zarudi, I., *et al.*, *Appl. Phys. Lett.* (2003) **82**, 1027
114. Zarudi, I., *et al.*, *Appl. Phys. Lett.* (2003) **82**, 874
115. Ge, D. B., *et al.*, *J. Appl. Phys.* (2003) **93**, 2418
116. Lloyd, S. J., *et al.*, *J. Mater. Res.* (2001) **16**, 3347
117. Lloyd, S. J., *et al.*, *Proc. R. Soc. A* (2005) **461**, 2521
118. Bradby, J. E., *et al.*, *Appl. Phys. Lett.* (2000) **77**, 3749
119. Patriarche, G., *et al.*, *J. Appl. Phys.* (2004) **96**, 1464
120. Pharr, G. M., *et al.*, *Scripta Mater.* (1989) **23**, 1949
121. Domnich, V., *et al.*, *Appl. Phys. Lett.* (2000) **76**, 2214
122. Domnich, V., and Gogotsi, Y., *Exp. Methods Phys. Sci.* (2001) **38**, 355
123. Tachi Suprijadi, M., *et al.*, *Philos. Mag. Lett.* (2002) **82**, 133